Strong SHG Responses in A Beryllium-Free Deep-UV-Transparent Hydroxyborate via Covalent Bond Modification

Chao Wu,[+a] Xingxing Jiang,[+b] Lin Lin,[a] Zheshuai Lin,[b] Zhipeng Huang,[a] Mark G. Humphrey,[c] and Chi Zhang*[a]

[a] Dr. C. Wu, L. Lin, Prof. Z. P. Huang, Prof. C. Zhang
China-Australia Joint Research Center for Functional Molecular Materials
School of Chemical Science and Engineering, Tongji University, Shanghai 200092, China
E-mail: chizhang@tongji.edu.cn
[b] Dr. X. X. Jiang, Prof. Z. S. Lin
Technical Institute of Physics and Chemistry
Chinese Academy of Sciences, Beijing 100190, China
[c] Prof. M. G. Humphrey
Research School of Chemistry, Australian National University
Canberra, ACT 2601, Australia
[+] C. Wu and X. X. Jiang contributed equally to the work

Supporting information for this article is given via a link at the end of the document.

Abstract: Deep-ultraviolet (deep-UV) nonlinear optical (NLO) crystals are key materials for creation of tunable deep-UV laser sources. However, practical application of the sole usable crystal, $KBe_2BO_3F_2$, has been hindered by the toxicity of beryllium and its layering tendency in crystal growth. Herein, we report a beryllium-free deep-UV NLO material $NaSr_3(OH)(B_9O_{16})[B(OH)_4]$ (NSBOH), synthesized by a covalent bond modification strategy under hydrothermal conditions. Moisture-stable NSBOH exhibits strong second-harmonic generation (SHG) at 1064 nm (3.3 × KH_2PO_4) and 532 nm (0.55 × β-BaB_2O_4), both amongst the largest powder SHG responses for a deep-UV borate, with good phase-matchability and a short wavelength cutoff edge (below 190 nm). NSBOH possesses a three-dimensional covalent anionic $[B_9O_{19}]_\infty$ honeycomb-like framework with no layering. The Sr^{2+} and Na^+ ions, residing in the cavities of the anionic framework, act as templates for the assembly and favorable alignment of the NLO-active groups, resulting in an optimal balance between strong SHG activities and wide UV transparency, and highlighting NSBOH as an attractive candidate for deep-UV NLO applications.

Introduction

Deep-ultraviolet (deep-UV) nonlinear optical (NLO)-active materials that are capable of generating coherent light at wavelengths below 200 nm through cascaded frequency conversion have attracted intense academic and technological interest for their promising applications in areas such as laser micromachining, photolithography, attosecond pulse generation, and advanced instrument development.[1] During the past decade, a number of NLO materials with crystallographic noncentrosymmetric structures, including metal carbonates,[2] nitrates,[3] phosphates,[4] sulfates,[5] fluorooxoborates[6] and especially borates,[7,8] have been explored for potential deep-UV applications. However, despite these advances, the development of new materials that are optically applicable in the deep-UV region remains a significant challenge. This is because of the often-competing structure requirements: large second-harmonic generation (SHG) response, high transparency in the deep-UV region, phase-matching capability, chemical stability, and ease of growth of large crystals.[9] At present, only $KBe_2BO_3F_2$ (KBBF)[10a] is potentially applicable in a practical sense in the deep-UV region. The structure-based superior optical properties of KBBF arise from the unique $[Be_2BO_3F_2]_\infty$ layers, in which NLO-active $[BO_3]^{3-}$ groups adopt a coplanar configuration with an aligned arrangement promoting SHG and birefringence.[10] Unfortunately, KBBF exhibits a layering tendency in single-crystal growth due to its weak interlayer bonding, while the need for highly toxic beryllium oxide powders in the synthesis and crystal growth remains a major obstacle to its broader technological application.[11] As a consequence, there is an urgent demand to develop the next generation of deep-UV NLO-active materials exhibiting superior crystal growth properties and devoid of toxic beryllium.

One successful strategy to overcome the structural disadvantages of KBBF is to strengthen interlayer interactions by introducing stronger B−O/Be−F bonds, the resultant deep-UV NLO borates including $Sr_2Be_2B_2O_7$,[7b] $Na_2CsBe_6B_5O_{15}$,[12a] $Na_2Be_4B_4O_{11}$,[12b] $LiNa_5Be_{12}B_{12}O_{33}$,[12b] $NaBeB_3O_6$,[12c] $ABe_2B_3O_7$ (A = K^+, Rb^+),[12c] and γ-Be_2BO_3F.[12d] Despite the improvement in layer growth, the optical properties of the resulting crystals are not as favorable as KBBF, while the use of toxic BeO remains a serious concern during synthesis. Another effective approach is to introduce metallic polyhedra into borates (e.g. Li^+, Zn^{2+}, Al^{3+}, etc), which increases the interlayer interactions and thereby improves the crystal growth habits. The reported beryllium-free deep-UV NLO borates[13] include β-$Rb_2Al_2B_2O_7$,[13a] $Li_4Sr(BO_3)_2$,[13b] $X_3Y_3Li_2Al_4B_6O_{20}F$ (X = K^+, Rb^+, Y = Ba^{2+}; X = K^+, Y = Sr^{2+}),[13c,13d,13e] $Rb_3Al_3B_3O_{10}F$,[13f] and $CsAlB_3O_6F$.[13g] However, these deep-UV NLO borates are usually synthesized via high-temperature solid-state reactions, a procedure that is unfavorable for large-scale preparation because of its high energy consumption. We were therefore prompted to explore the synthesis of beryllium-free, good crystal-growth habit, deep-UV NLO crystals under mild conditions.[14]

In 2011, Chen reported the deep-UV NLO material $NaSr_3Be_3B_3O_9F_4$ (NSBBOF),[15] which was obtained via a high-temperature melting method. The arrangement of the $[Be_3B_3O_{12}F]^{10-}$ primary building units (PBUs) is favorable for generating excellent optical properties (including large NLO response and moderate birefringence), and for avoiding layering

during bulk crystal growth. Unfortunately, the toxic beryllium has hindered the practical application of this material. Since nonmetallic anion tetrahedra (e.g. $[BO_4]^{5-}$, $[PO_4]^{3-}$, and $[SiO_4]^{4-}$)[16] possess similar coordination geometries to the beryllium-containing $[BeO_3F]^{5-}$ unit, in principle they can be introduced into functional structures by replacing the beryllium-centered tetrahedra. We therefore propose a covalent bond modification strategy to create new beryllium-free borates that are based on the NSBBOF structure drawing on three specific ideas: (i) the replacement of $[BeO_3F]^{5-}$ by $[BO_4]^{5-}$ units can remove the toxic beryllium that is present in NSBBOF. The PBU in the new structure should exhibit differing connectivity to that of the $[Be_3B_3O_{12}F]^{10-}$ PBU in NSBBOF because of the covalently bonded B−O−B bridges, which enhance the prospects of forming a 3D covalent B-O framework and minimize the tendency for layering; (ii) the flexible coordination environments of the $[BO_3]^{3-}$ and $[BO_4]^{5-}$ units[17] may promote retention by the resultant PBU of the configuration of the parent $[Be_3B_3O_{12}F]^{10-}$ PBU, for which the three six-membered rings play a key role in engineering the desirable linear and nonlinear optical responses; iii) the nonbonding O 2*p* orbitals may be eliminated when the covalently bonded $[BO_3]^{3-}$/$[BO_4]^{5-}$ units are oligomerized to form the boron-rich PBUs, and this is expected to lead to a large bandgap and thereby wide UV transparency.

In this work, we report the facile hydrothermal synthesis of $NaSr_3(OH)(B_9O_{16})[B(OH)_4]$ (NSBOH) through the substitution of the $[BeO_3F]^{5-}$ units in the $[Be_3B_3O_{12}F]^{10-}$ PBUs of NSBBOF with the homovalent nonmetallic $[BO_4]^{5-}$ units. Consistent with the aforementioned propositions, the noncentrosymmetric NSBOH exhibits strong phase-matchable SHG efficiencies of 3.3 times that of KH_2PO_4 (KDP) at 1064 and 0.55 times that of β-BaB_2O_4 (BBO) at 532 nm with a deep-UV cutoff edge below 190 nm, both amongst the largest powder SHG responses for a deep-UV borate. It is noteworthy that, although a number of NCS hydroxyborates have been reported, UV/deep-UV SHG-efficient hydroxyborates are thus far little exploited. Density functional theory (DFT) calculations on NSBOH reveal that the good balance achieved between SHG response and UV transparency can be attributed to the synergistic influence of the $[B_9O_{19}]^{11-}$ and $[BO_4]^{5-}$ units.

Results and Discussion

NSBOH is the first noncentrosymmetric (NCS) sodium strontium borate. It crystallizes in the polar space group $P3_1c$ and exhibits a three-dimensional (3D) structure consisting of an anionic $[B_9O_{19}]_\infty$ honeycomb-like framework with Sr^{2+} and Na^+ cations and $[B(OH)_4]^-$ anions residing in the channels (Tables S1 and S2, and Figure 1d). The C_3 symmetric PBU $[B_9O_{19}]^{11-}$ is comprised of six $[BO_4]^{5-}$ tetrahedra (T) sharing oxygen vertices and three $[BO_3]^{3-}$ triangles (Δ) attached to the terminal vertices of these tetrahedra (Figures 1a, 1b), which can be written as [9:(3Δ + 6T)]. Each $[B_9O_{19}]^{11-}$ PBU is covalently bonded to six other neighboring PBUs through B−O−B bridges (Figure 1e). This spatial arrangement presumably contributes to the weak layering tendency, and thereby facilitates the crystal growth process.[15a] The $[B_9O_{19}]^{11-}$ PBUs connect to each other to construct a 3D framework with six-membered ring channels along the *c*-axis (Figure S1a). The disordered $[B(3)O_4]^{5-}$ tetrahedra are encapsulated in the channels (Figure 1d). The anionic framework possesses an *acs* net topology ($4^9{\cdot}6^6$) with six-connected nodes

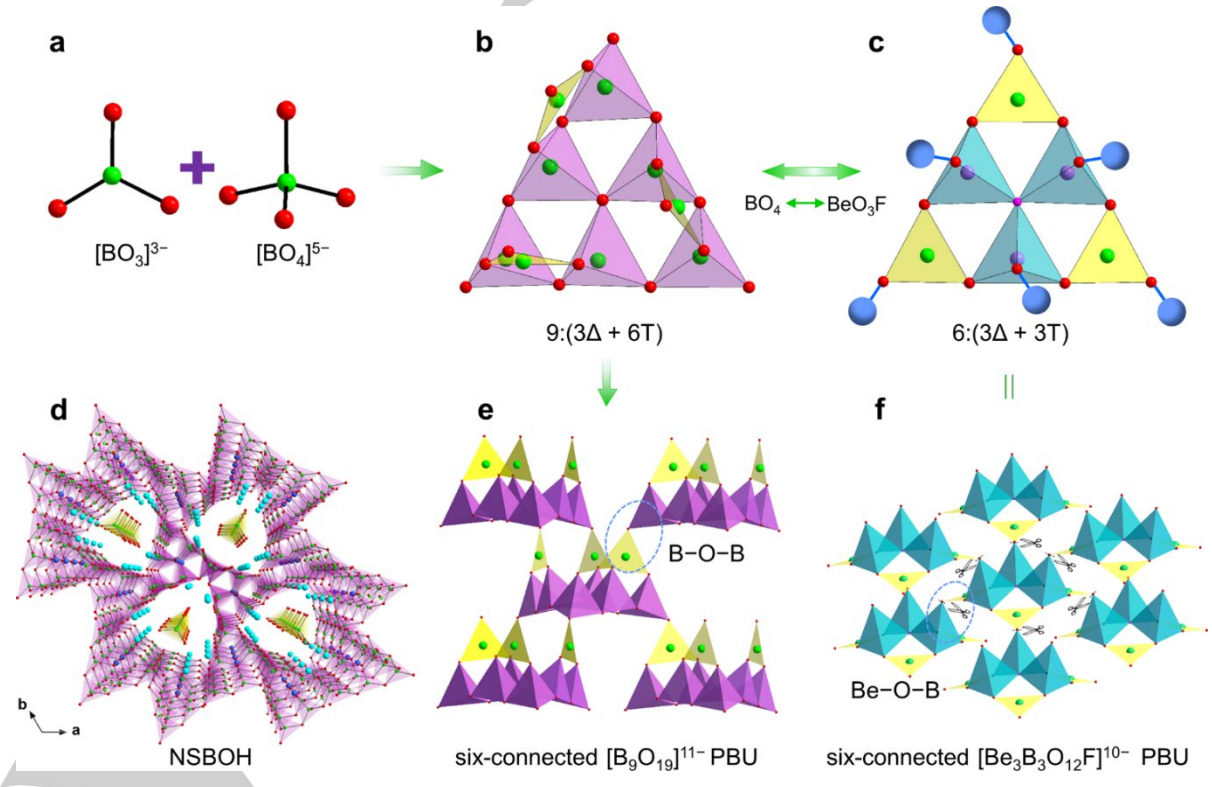

Figure 1. (a) The $[BO_3]^{3-}$ and $[BO_4]^{5-}$ units. (b) The $[B_9O_{19}]^{11-}$ PBU. (c) The $[Be_3B_3O_{12}F]^{10-}$ PBU in $NaSr_3Be_3B_3O_9F_4$. Adjacent $[Be_3B_3O_{12}F]^{10-}$ are simplified as large blue balls. (d) Perspective view of the 3D framework of NSBOH along the *c*-axis, with the Sr−O and Na−O bonds omitted for clarity. (e) Polyhedral linking mode of the $[B_9O_{19}]^{11-}$ PBU of NSBOH and six adjacent PBUs. (f) Polyhedral linking mode of the $[Be_3B_3O_{12}F]^{10-}$ PBU of $NaSr_3Be_3B_3O_9F_4$ and six adjacent PBUs. Colour codes: green for B, red for O, turquoise for Sr, light blue for Na, lavender for Be, pink for F.

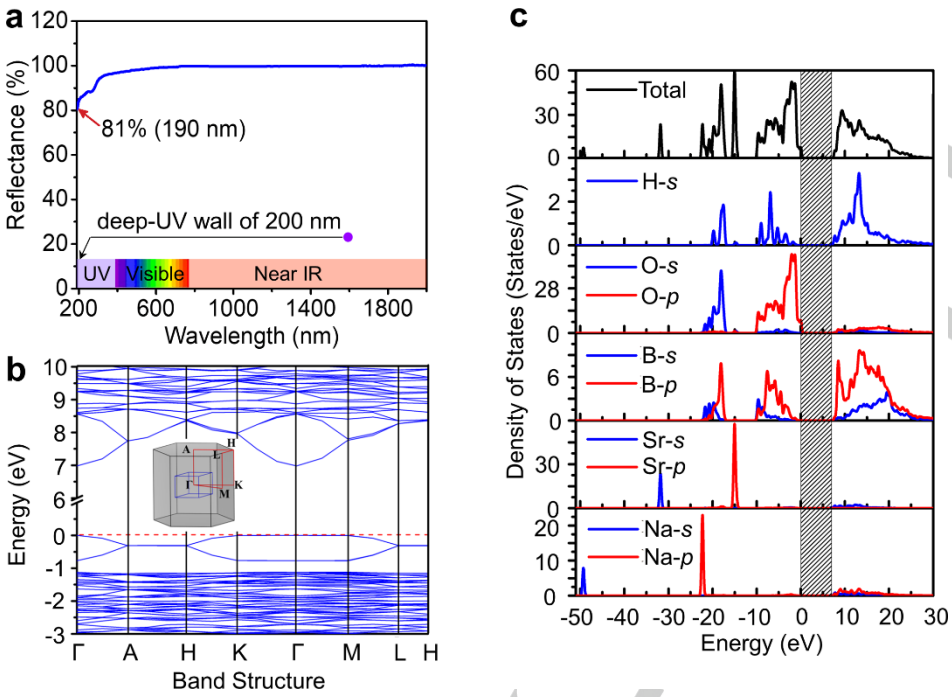

Figure 2. (a) UV-Vis-NIR diffuse reflectance spectrum of NSBOH. (b) Electronic band structure along a highly symmetrical path in the Brillouin zone of NSBOH. (c) Density of states (DOS) projected onto the constituent atoms of NSBOH. The forbidden bands are highlighted by striped hatching.

(Figure S1b). The connectivity of the Sr−O and Na−O bonds leads to a 3D honeycomb-like cationic framework consisting of $[NaSr_3O_{28}]_\infty$ units (Figure S2), which interpenetrate the abovementioned 3D anionic framework by sharing both O vertices and O−O edges.

The Sr^{2+} cations are surrounded by ten oxygen atoms with Sr−O distances of 2.407(7)−3.028(3) Å, while the Na^+ cations are coordinated by seven oxygen atoms with Na−O distances in the range 2.200(6)−2.480(4) Å. There are four crystallographically independent boron atoms: B(4) is coordinated to three O atoms, forming a nearly planar $[BO_3]^{3-}$ unit with B−O bond lengths varying from 1.359(6) to 1.385(6) Å and O−B−O bond angles from 116.2(4)−122.0(4)° with a mean value of about 120°, while B(1), B(2) and B(3) all coordinate to four O atoms in a tetrahedral manner with B−O bond lengths and O−B−O bond angles ranging from 1.338(7)−1.572(13) Å and 106.4(4)−119.46(17)°, respectively. The bond valence calculations[18] (Na, 1.48; Sr, 2.09; B 2.97−3.05) are consistent with formal oxidation states of 1+ for Na, 2+ for Sr, and 3+ for B (Table S3).

From the viewpoint of structural evolution, NSBOH can be regarded as a derivative of NSBBOF. The two structures exhibit similar PBUs (Figures 1b, 1c), with the $[BeO_3F]^{5-}$ tetrahedra in the $[Be_3B_3O_{12}F]^{10-}$ PBU of NSBBOF being replaced by $[BO_4]^{5-}$ tetrahedra in NSBOH, creating $[B_6O_{16}]^{14-}$ units that are capped on one side by three $[BO_3]^{3-}$ units. The resultant $[B_9O_{19}]^{11-}$ PBUs in NSBOH possess the same six-connected linking mode as $[Be_3B_3O_{12}F]^{10-}$ in NSBBOF (Figures 1e, 1f). This structural evolution affords several beneficial characteristics: (1) the replacement of $[BeO_3F]^{5-}$ by the $[BO_4]^{5-}$ tetrahedra removes the toxic beryllium that is present in NSBBOF; (2) the structure of the derivative NSBOH not only preserves the NLO-favorable structural $[BO_3]^{3-}$ units along the *c*-axis, but also introduces an ordered arrangement of $[BO_4]^{5-}$ units in the *ab* plane, which is expected to produce a sizable SHG response and birefringence (Figure S1a); (3) unlike the Be−O−B bridged connectivity mode of the $[Be_3B_3O_{12}F]^{10-}$ PBU, each $[B_9O_{19}]^{11-}$ PBU in NSBOH is connected to six neighboring PBUs along the *c*-axis via covalently bonded B−O−B bridges. This is also in sharp contrast to the weak interlayer K−F ionic bonds in KBBF, the spatial arrangement and covalent bond connection in NSBOH are expected to reduce the layering tendency and to promote bulk crystal growth.

Thermogravimetric analysis (TGA) shows that NSBOH is thermally stable up to 350 °C (Figure S3), with the 6.05% weight loss in the range 350−670 °C corresponding closely to the calculated value for 2.5 H_2O molecules (6.13%). The moisture-stability of NSBOH was also examined. Crystals were exposed to air for six months or soaked in water for two weeks, both at room temperature; the crystals maintained their transparency (Figure S4), while the powder X-ray diffraction (XRD) peaks of the crystals exposed to air or soaked in water are in good agreement with the simulated powder XRD pattern of NSBOH (Figure S5). The SHG intensity of NSBOH in the particle size range 105−150 μm was also measured after exposure to air for six months or soaking in water for two weeks, no obvious difference between the SHG intensities of the sample before and after the exposure or soaking processes being seen (Figure 3c). The IR spectrum of NSBOH is shown in Figure S6. Bands are seen at 1250−1500 cm^{-1} ($[BO_3]^{3-}$ groups) and 850−1140 cm^{-1} ($[BO_4]^{5-}$ groups), with bands around 500−780 cm^{-1} likely to stem from bending vibrations of the $[BO_3]^{3-}$ and $[BO_4]^{5-}$ groups, and a broad band from the $[OH]^-$ groups at ca. 3400 cm^{-1}.

The room-temperature UV-Vis-NIR diffuse reflectance spectrum reveals that the reflectance of NSBOH in the range 190−2000 nm is above 81%, with a short-wavelength UV cutoff edge below 190 nm (Figure 2). No obvious absorption peak was observed for NSBOH in the range 0.62–6.53 eV, indicating that the experimental band gap value is greater than 6.53 eV, confirming that NSBOH possesses transparency that extends into the deep-UV. To shed further light on the microscopic mechanism of the optical properties of NSBOH, first-principles calculations based on density functional theory (DFT) were

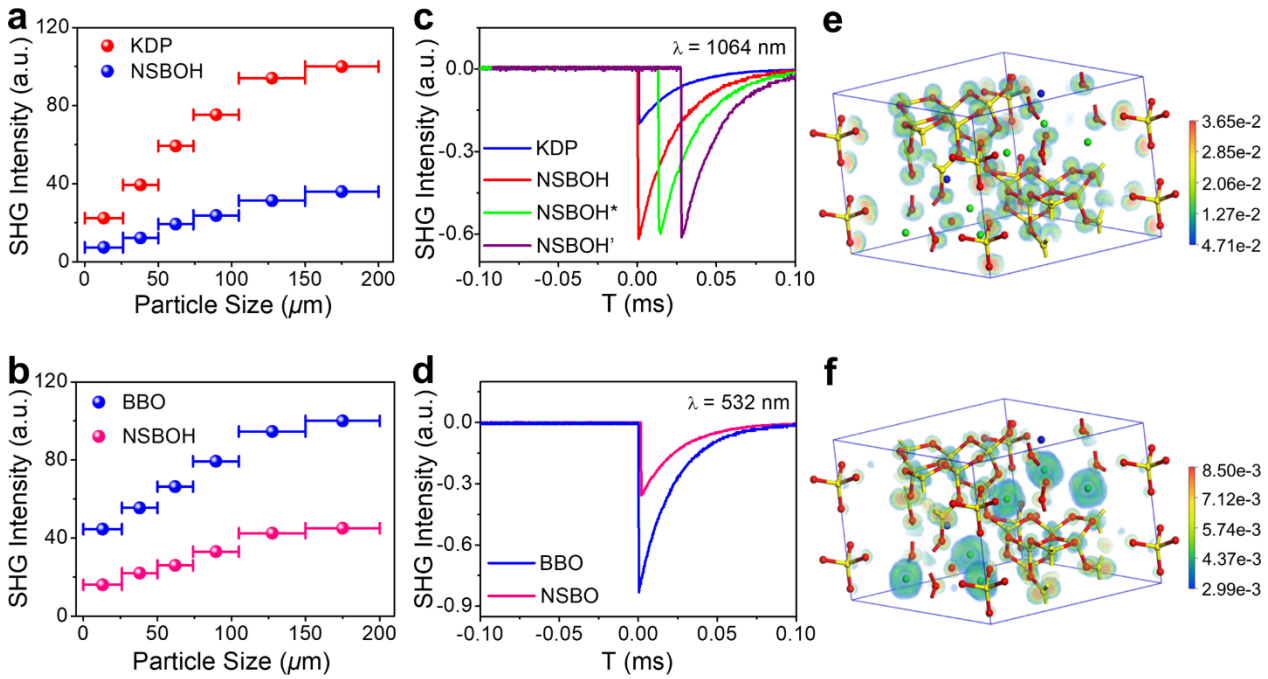

Figure 3. Phase-matching curves of NSBOH with 1064 nm (a) and 532 nm (b) laser radiation. Oscilloscope traces of the SHG signals of NSBOH (105−150 μm), NSBO* (following exposure to air for six months), and NSBO' (following soaking in water for a week) with 1064 nm (c) and 532 nm (d) laser radiation. KDP and BBO were used as references for the SHG measurements at 1064 and 532 nm, respectively. SHG-weighted electron densities of the (c) occupied and (d) unoccupied orbitals. Color codes: gold for B, red for O, green for Sr, blue for Na. Hydrogen atoms have been omitted for clarity.

performed.[19] The band structure (Figure 2b) reveals that the valence band maximal (VBM) and conduction band minimal (CBM) are located at the same point (Γ), resulting in a direct band gap of 6.98 eV (corresponding to 178 nm). Figure 2c displays the density of states (DOS) and the partial density of states (PDOS) projected on the constituent atoms, from which several electronic characteristics can be deduced: (i) Na 2*s*, Sr 4*s* and Na 2*p* orbitals are overwhelmingly localized at the inner-shell states around -51 eV, -32 eV and -22 eV, respectively. It is difficult to excite these electrons by the external perturbation of a weak electric field, and so they contribute almost nothing to the optical properties related to electronic transition across the forbidden bands. (ii) B 2*s* and 2*p* and O 2*p* orbitals span the range -22 eV to -15 eV, the strong hybridization between these orbitals implying a strong covalent interaction within the $[BO_4]^{5-}$ and $[B_9O_{19}]^{11-}$ groups. (iii) The sharp peak of the Sr 4*p* orbitals occurs at -15 eV, and this is only weakly hybridized with other orbitals, manifesting the strong ionicity of the Sr atoms. (iv) The top of the VB (-10 eV to 0 eV) and bottom of the CB (6.98 eV to 20 eV) are predominantly occupied by B 2*p* and O 2*p* orbitals. It should be emphasized that the optical properties of NSBOH are mainly determined by the behaviour of the electrons near the band gap, so it can therefore be concluded that the $[BO_4]^{5-}$ and $[B_9O_{19}]^{11-}$ groups are the main contributors to the optical response.

As NSBOH crystallizes with a noncentrosymmetric structure, we then examined its SHG properties. The powder frequency-doubling merit was assessed by the Kurtz and Perry method[20] employing a Q-switched Nd:YAG laser at the fundamental wavelength of 1064 nm and the frequency-doubled wavelength of 532 nm for visible and UV SHG, respectively. The curves of the SHG signals as a function of particle size were recorded using sieved KDP and BBO as references with the same particle size ranges. As shown in Figures 3a, 3b, the SHG intensity of NSBOH increases with increasing particle size, indicating that the crystalline material exhibits phase-matching in both the visible and UV regions. Interestingly, the phase-matching capability of NSBOH extends into the middle-to-far UV region (*e.g.*, SHG@532 nm), which is rare for NLO hydroxyborates.[1d] The SHG efficiency of NSBOH was found to be approximately 3.3 × KDP@1064 nm and 0.55 × BBO@532 nm, respectively, in the 105−150 μm particle size range (Figures 3c, 3d), both values being amongst the largest efficiencies for reported deep-UV NLO borates. The SHG efficiency of NSBOH is significantly larger than those of the deep-UV beryllium borates KBBF (1.2 × KDP),[10a] $Na_2CsBe_6B_5O_{15}$ (1.17 × KDP),[12a] $Na_2Be_4B_4O_{11}$ (1.30 × KDP)[12b] and $LiNa_5Be_{12}B_{12}O_{33}$ (1.4 × KDP),[12b] and the deep-UV beryllium-free borates $Li_4Sr(BO_3)_2$

Table 1. Selected beryllium-free NLO borates with deep-UV cutoff edges.

Compound	Space group	UV cutoff edge (nm)	SHG response
β-BaB_2O_4[7a]	*R*3*c*	189	5.8
$Li_4Sr(BO_3)_2$[13b]	*Cc*	186	2[b] / 0.3[c]
β-$Rb_2Al_2B_2O_7$[13a]	*P*3$_2$1	<200	2[b] / 0.4[c]
$K_3Ba_3Li_2Al_4B_6O_{20}F$[13c]	*P*-62*c*	190	1.5
$Ba_4B_{11}O_{20}F$[21a,b]	*Cmc*2$_1$	175	4
$Rb_3Al_3B_3O_{10}F$[13f]	*P*3$_1$*c*	<200 (188[a])	1.2
$Ba_3Mg_3(BO_3)_3F_3$[21c]	*Pna*2$_1$	184	1.8
$Ba_3Mg_3(BO_3)_3F_3$[21c]	*P*-62*m*	184	2
$CsZn_2BO_3Cl_2$[8a]	*R*32	<190	2.8
CsB_4O_6F[6d]	*Pna*2$_1$	155	1.9[b] / 0.35[c]
$NH_4B_4O_6F$[8a]	*Pna*2$_1$	156	3[b] / 0.5[c]
$SrB_5O_7F_3$[6a]	Cmc2$_1$	<180	1.6[b] / 0.5[c]
$SrB_8O_{15}H_4$[9a]	*P*2$_1$	<200 (176[a])	2.2
$CaB_8O_{15}H_4$[9a]	*P*2$_1$	<200 (165[a])	1.8
NSBOH (this work)	*P*3$_1$*c*	<190 (176[a])	3.3[b] / 0.55[c]

[a]DFT calculated results. [b]SHG response at 1064 nm with KDP as the reference. [c]SHG response at 532 nm with BBO as the reference.

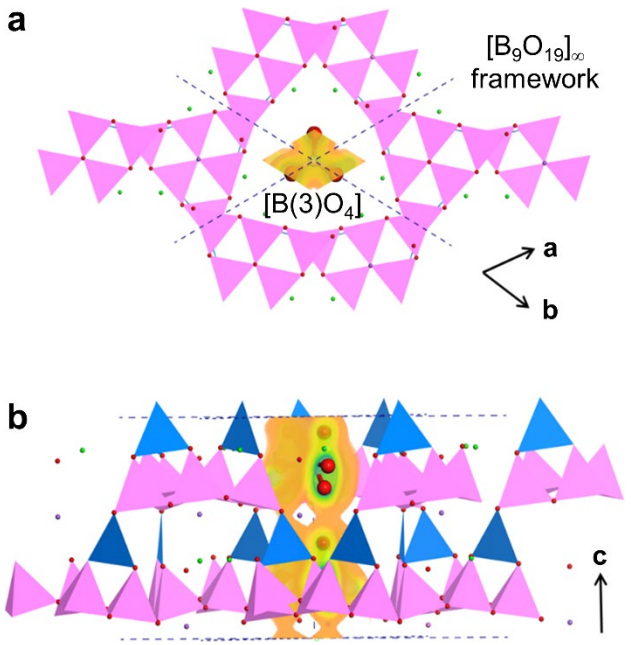

Figure 4. Electron density distribution of the disordered $[B(3)O_4]^{5-}$ groups in the channel of $[B_9O_{19}]_\infty$ framework. (a) Top view, (b) Side view.

(2.0 × KDP),[13b] $K_3Ba_3Li_2Al_4B_6O_{20}F$ (1.5 × KDP),[13c] and $Rb_3Al_3B_3O_{10}F$ (1.2 × KDP),[13f] and is comparable to those of the deep-UV borates $NaSr_3Be_3B_3O_9F_4$ (4.0 × KDP)[15a] and $Ba_4B_{11}O_{20}F$ (4.0 × KDP)[21b] (Table 1), which were prepared under conventional high-temperature solid-state conditions.

To determine the origin of the strong SHG response, quantitative calculations were carried out on the dipole moments of the $B(3)O_4$, $B(4)O_3$, SrO_{10}, and NaO_7 groups of NSBOH using a bond valence approach (Table S4).[22] The magnitudes of the dipole moments along the *a*- and *b*-axes cancel while their vector sum is significantly enhanced along the *c*-axis. The experimental results were also supported by first-principles calculations. From the space group ($P3_1c$) and Kleinman symmetry,[23] NSBOH has three independent SHG tensor components (d_{22}, d_{31}, d_{33}). The SHG coefficients of d_{22}, d_{31}, and d_{33} calculated by the length-gauge formalism[24] are 0.28 pm/V, 0.51 pm/V, and 0.90 pm/V, respectively. The largest, d_{33}, was ca. 2.3 times that of KDP (0.39 pm·V^{-1}), which agrees well with the experimental measurements. An SHG-weighted electron density analysis[25] was performed to give an intuitive indication of the microscopic electronic origin, and in particular to highlight the occupied and unoccupied orbitals vital to the SHG effect in NSBOH (Figures 4e and 4f). This analysis reveals that the SHG-active electron clouds for both the occupied and unoccupied orbitals are predominantly located on the $[BO_4]^{5-}$ and $[B_9O_{19}]^{11-}$ groups, although a small part of the unoccupied SHG densities are found at the Sr sites. The large

Table 2. Calculated nonlinear optical properties for $NaSr_3(OH)(B_9O_{16})[B(OH)_4]$ deduced from real-space atom-cutting analysis[a]

	d_{22}	d_{31}	d_{33}
all	0.28	0.51	0.90
Na^+	0.01	0.03	-0.02
Sr^{2+}	0.03	0.02	0.06
$[B(OH)_4]^-$	0.09	0.10	0.18
$[B_9O_{19}]^{11-}$	0.32	0.68	1.11

[a] *d* values in pm/V.

SHG response in NSBOH can therefore be mainly ascribed to the virtual electronic transitions inside the $[BO_4]^{5-}$ and $[B_9O_{19}]^{11-}$ groups. A real-space atom cutting method was also employed to more quantitatively identify the contribution from the respective units (or ions) (Table 2). Several observations can be made: (1) The contributions of the Na^+ and Sr^{2+} cations are negligible, which can be attributed to the spherical distribution of their electron clouds. (2) The $[B_9O_{19}]^{11-}$ units make the dominant contribution (more than 70%) to the SHG response in NSBOH, consistent with the delocalized electron clouds observed in the SHG-weighted electron density map. (3) The $[B(OH)_4]^-$ units account for only about 14% of the largest SHG coefficient d_{33}. In contrast to the $[B_9O_{19}]^{11-}$ units, the electron density around the $[B(OH)_4]^-$ units is localized. These results demonstrate that the SHG contribution of the $[B_9O_{19}]^{11-}$ units is larger than that of the $[B(OH)_4]^-$ units under the perturbation of ambient optoelectronic fields.

The dispersions of the linear refractive indices for this crystal were calculated, and NSBOH is a negative uniaxial crystal with birefringence Δn = 0.0386 at 1064 nm. The powder SHG measurement indicates NSBOH shows good phase-matchability in the near deep-UV region. Our calculations reveal that the optical birefringence for phase-matching mainly results from the disordered $[B(3)O_4]^{5-}$ groups encapsulated in the $[B_9O_{19}]_\infty$ channels, which produce a condensed electron density distribution along the *c*-axis (Figure 4), and thus have a strong anisotropy for optical response.

Conclusion

In summary, a noncentrosymmetric polar sodium strontium hydroxyborate, $NaSr_3(OH)(B_9O_{16})[B(OH)_4]$, was constructed by a covalent bond modification strategy based on the model structure NSBBOF via a facile hydrothermal reaction. NSBOH possesses a 3D anionic $[B_9O_{19}]_\infty$ honeycomb-like framework, with Sr^{2+} and Na^+ cations and $[B(OH)_4]^-$ anions residing in the cavities. Chemically-stable crystalline NSBOH is SHG active at both 1064 nm and 532 nm, with deep-UV transparency to wavelengths as short as 190 nm, and good phase-matchability in the near deep-UV region, a rare combination for NLO borates. NSBOH additionally exhibits strong SHG efficiencies (3.3 × KDP@1064 nm, 0.55 × BBO@532 nm), both amongst the largest powder SHG responses for all deep-UV borates thus far. This strategy therefore successfully resolves the strong SHG response/deep-UV transparency dichotomy. Density functional theory (DFT) calculations combined with a dipole moment study were employed to rationalize the optical properties. The origin of the enhanced SHG response can be attributed to coplanar, better aligned NLO-active groups. This work demonstrates that NSBOH is a promising deep-UV NLO crystal, and that the covalent bond modification strategy provides a feasible approach to the development of novel beryllium-free non-layered high-performance deep-UV NLO crystals.

Acknowledgements

This research was financially supported by the National Natural Science Foundation of China (No. 51432006), the Ministry of Education of China for the Changjiang Innovation Research Team (No. IRT14R23), the Ministry of Education and the State Administration of Foreign Experts Affairs for the 111 Project (No. B13025), and the Innovation Program of Shanghai Municipal Education Commission. M.G.H. thanks the Australian Research Council for support (DP170100411). C.W. thanks the National and Shanghai Postdoctoral Program for Innovative Talents (nos. BX201800216 and 2018192).

Keywords: borates • hydrothermal synthesis • deep-ultraviolet • second-harmonic generation • structure–property relationships

[1] a) N. Savage, *Nat. Photonics* **2007**, *1*, 83-85; b) D. Cyranoski, *Nature* **2009**, *457*, 953-955; c) M. Mutailipu, M. Zhang, Z. H. Yang, S. L. Pan, *Acc. Chem. Res.* **2019,** *52*, 791-801; d) C. Wu, G. Yang, M. G. Humphrey, C. Zhang, *Coord. Chem. Rev*. **2018**, *375*, 459-488.

[2] a) X. M. Liu, L. Kang, P. F. Gong, Z. S. Lin, *Angew. Chem. Int. Ed.* **2021**, *60*, 13574-13578; *Angew. Chem.* **2021**, *133*, 13686-13690; b) T. T. Tran, J. Young, J. M. Rondinelli, P. S. Halasyamani, *J. Am. Chem. Soc.* **2017,** *139*, 1285-1295; c) G. Peng, C. C. Lin, N. Ye, *J. Am. Chem. Soc.* **2020**, *142*, 20542-20546.

[3] a) X. M. Liu, P. F. Gong, Y. Yang, G. M. Song, Z. S. Lin, *Coord. Chem. Rev.* **2019**, *400*, 213045; b) L. Huang, G. H. Zou, H. Q. Cai, S. C. Wang, C. S. Lin, N. Ye, *J. Mater. Chem. C* **2015**, *3*, 5268-5274; c) C. Wu, X. X. Jiang, Z. J. Wang, L. Lin, Z. S. Lin, Z. P. Huang, X. F. Long, M. G. Humphrey, C. Zhang, *Angew. Chem. Int. Ed.* **2021**, *60*, 3464-3468; *Angew. Chem.* **2021**, *133*, 3506-3510.

[4] a) L. Li, Y. Wang, B. H. Lei, S. J. Han, Z. H. Yang, K. R. Poeppelmeier, S. L. Pan, *J. Am. Chem. Soc.* **2016**, *138*, 9101-9104; b) S. G. Zhao, P. F. Gong, S. Y. Luo, L. Bai, Z. S. Lin, Y. Y. Tang, Y. L. Zhou, M. C. Hong, J. H. Luo, *Angew. Chem. Int. Ed.* **2015**, *54*, 4217-4221; *Angew. Chem.* **2015**, *127*, 4291-4295; c) X. F. Lu, Z. H. Chen, X. R. Shi, Q. Jing, M. H. Lee, *Angew. Chem. Int. Ed.* **2020**, *59*, 17648-17656; *Angew. Chem.* **2020**, *132*, 17801-17809; d) J. Chen, L. Xiong, L. Chen, L. M. Wu, *J. Am. Chem. Soc.* **2018**, *140*, 14082-14086; e) C. Wu, X. X. Jiang, Z. J. Wang, H. Y. Sha, Z. S. Lin, Z. P. Huang, X. F. Long, M. G. Humphrey, C. Zhang, *Angew. Chem. Int. Ed.* **2021**, *60*, 14806-14810; *Angew. Chem.* **2021**, *133*, 14932-14936.

[5] a) Y. Q. Li, F. Liang, S. G. Zhao, L. N. Li, Z. Y. Wu, Q. R. Ding, S. Liu, Z. S. Lin, M. C. Hong, J. H. Luo, *J. Am. Chem. Soc.* **2019**, *141*, 3833-3837; b) X. H. Dong, L. Huang, C. F. Hu, H. M. Zeng, Z. E. Lin, X. Wang, K. M. Ok, G. H. Zou, *Angew. Chem. Int. Ed.* **2019**, *58*, 6528-6534; *Angew. Chem.* **2019**, *131*, 6598-6604; c) C. Wu, T. H. Wu, X. X. Jiang, Z. J. Wang, H. Y. Sha, L. Lin, Z. S. Lin, Z. P. Huang, X. F. Long, M. G. Humphrey, C. Zhang, *J. Am. Chem. Soc.* **2021**, *143*, 4138-4142.

[6] a) M. Mutailipu, M. Zhang, B. B. Zhang, L. Y. Wang, Z. H. Yang, X. Zhou, S. L. Pan, *Angew. Chem. Int. Ed.* **2018**, *57*, 6095-6099; *Angew. Chem.* **2018**, *130*, 6203-6207; b) B. B. Zhang, G. Q. Shi, Z. H. Yang, F. F. Zhang, S. L. Pan, *Angew. Chem. Int. Ed.* **2017**, *56*, 3916-3919; *Angew. Chem.* **2017**, 129, 3974-3977; c) M. Luo, F. Liang, Y. Song, D. Zhao, F. Xu, N. Ye, Z. S. Lin, *J. Am. Chem. Soc.* **2018**, *140*, 3884-3887; d) X. F. Wang, Y. Wang, B. B. Zhang, F. F. Zhang, Z. H. Yang, S. L. Pan, *Angew. Chem. Int. Ed.* **2017**, *56*,14119-14123; *Angew. Chem.* **2017**, *129*, 14307-14311.

[7] a) C. T. Chen, B. C. Wu, A. D. Jiang, G. M. You, *Sci. Sin., Ser. B* **1985**, *28*, 235-243; b) C. T. Chen, Y. B. Wang, B. C. Wu, K. C. Wu, W. L. Zeng, L. H. Yu, *Nature* **1995**, *373*, 322-324; c) C. T. Chen, Y. C. Wu, A. D. Jiang, B. C. Wu, G. M. You, R. K. Li, S. J. Lin, *J. Opt. Soc. Am. B* **1989**, *6*, 616-621.

[8] a) G. Q. Shi, Y. Wang, F. F. Zhang, B. B. Zhang, Z. H. Yang, X. L. Hou, S. L. Pan, K. R. Poeppelmeier, *J. Am. Chem. Soc.* **2017**, *139*, 10645-10648; b) J. J. Zhou, Y. Q. Liu, H. P. Wu, H. W. Yu, Z. S. Lin, Z. G. Hu, J. Y. Wang, Y. C. Wu, *Angew. Chem. Int. Ed.* **2020**, *59*, 19006-19010; *Angew. Chem.* **2020**, *132*, 19168-19172; c) P. S. Halasyamani, J. M. Rondinelli, *Nat. Commun*. **2018**, *9*, 2972.

[9] a) P. F. Gong, L. Kang, Z. S. Lin, *J. Am. Chem. Soc.* **2020**, *142*, 15157-15163; b) H. W. Yu, W. G. Zhang, J. Young, J. M. Rondinelli, P. S. Halasyamani, *Adv. Mater.* **2015,** *27*, 7380-7385.

[10] a) C. T. Chen, G. L. Wang, X. Y. Wang, Z. Y. Xu, *Appl. Phys. B: Lasers Opt.* **2009**, *97*, 9-25; b) G. H. Zou, C. S. Lin, H. Jo, G. Nam, T. S. You, K. M. Ok, *Angew. Chem. Int. Ed.* **2016,** *55*, 12078-12082; Angew. Chem. **2016**, *128*, 12257-12261.

[11] H. W. Yu, N. Z. Koocher, J. M. Rondinelli, P. S. Halasyamani, *Angew.Chem. Int. Ed.* **2018**, *57*, 6100-6103; *Angew. Chem.* **2018**, *130*, 6208-6211.

[12] a) S. C. Wang, N. Ye, *J. Am. Chem. Soc.* **2011,** *133*, 11458-11461; b) H. W. Huang, L. J. Liu, S. F. Jin, W. J. Yao, Y. H. Zhang, C. T. Chen, *J. Am. Chem. Soc.* **2013,** *135*, 18319-18322; c) S. C. Wang, N. Ye, W. Li, D. Zhao, *J. Am. Chem. Soc.* **2010**, *132*, 8779-8786; d) G. Peng, N. Ye, Z. S. Lin, L. Kang, S. L. Pan, M. Zhang, C. S. Lin, X. F. Long, M. Luo, Y. Chen, Y. H. Tang, F. Xu, T. Yan, *Angew. Chem. Int. Ed.* **2018,** *57*, 8968-8972; *Angew. Chem.* **2018**, *130*, 9106-9110.

[13] a) T. T. Tran, N. Z. Koocher, J. M. Rondinelli, P. S. Halasyamani, *Angew. Chem. Int. Ed.* **2017,** *56*, 2969-2973; *Angew. Chem.* **2017**, *129*, 3015-3019; b) S. G. Zhao, P. F. Gong, L. Bai, X. Xu, S. Q. Zhang, Z. H. Sun, Z. S. Lin, M. C. Hong, C. T. Chen, J. H. Luo, *Nat. Commun.* **2014,** *5*, 4019; c) S. G. Zhao, L. Kang, Y. G. Shen, X. D. Wang, M. A. Asghar, Z. S. Lin, Y. Y. Xu, S. Y. Zeng, M. C. Hong, J. H. Luo, *J. Am. Chem. Soc.* **2016**, *138*, 2961-2964. d) H. W. Yu, J. Young, H. P. Wu, W. G. Zhang, J. M. Rondinelli, P. S. Halasyamani, *Adv. Opt. Mater.* **2017**, *5*, 1700840; e) H. P. Wu, H. W. Yu, S. L. Pan, P. S. Halasyamani, *Inorg. Chem.* **2017,** *56*, 8755-8758; f) S. G. Zhao, P. F. Gong, S. Y. Luo, S. J. Liu, L. N. Li, M. A. Asghar, T. Khan, M. C. Hong, Z. S. Lin, J. H. Luo, *J. Am. Chem. Soc.* **2015**, *137*, 2207-2210; g) H. K. Liu, Y. Wang, B. B. Zhang, Z. H. Yang, *Chem. Sci.* 2020, 11, 694-698.

[14] C. Wu, L. H Li, J. L. Song, G. Yang, M. G. Humphrey, C. Zhang, *Inorg. Chem.* **2017,** *56*, 1340-1348.

[15] a) H. W. Huang, J. Y. Yao, Z. S. Lin, X. Y. Wang, R. He, W. J. Yao, N. X. Zhai, C. T. Chen, *Angew. Chem. Int. Ed.* **2011,** *50*, 9141-9144; *Angew. Chem.* **2011**, *123*, 9307-9310; b) X. S. Wang, L. J. Liu, X. Y. Wang, L. Bai, C. T. Chen, *CrystEngComm* **2015**, *17*, 925-929.

[16] a) H. P. Wu, B. B. Zhang, H. W. Yu, Z. G. Hu, J. Y. Wang, Y. C. Wu, P. S. Halasyamani, *Angew. Chem. Int. Ed.* **2020**, *59*, 8922-8926; *Angew. Chem.* **2020**, *132*, 9007-9011; b) J. H. Huang, C. C. Jin, P. L. Xu, P. F. Gong, Z. S. Lin, J. W. Cheng, G. Y. Yang, *Inorg. Chem.* **2019**, *58*, 1755-1758; c) X. D. Zhang, L. C. Guo, B. B. Zhang, J. Yu, Y. Wang, K. Wu, H. J. Wang, M. H. Lee, *Chem. Commun.* **2021**, *57*, 639-642; d) B. L. Wu, C. L. Hu, F. F. Mao, R. L. Tang, J. G. Mao, *J. Am. Chem. Soc.* **2016**, *323*, 36-51; e) C. Wu, L. H. Li, G. Yang, J. L. Song, B. Yan, M. G. Humphrey, L. Zhang, J. Shao, C. Zhang, *Dalton Trans.* **2017,** *46*, 12605-12611.

[17] a) D. Vitzthum, K. Wurst, J. M. Pann, P. Brüggeller, M. Seibald, H. Huppertz, *Angew. Chem. Int. Ed.* **2018**, *57*, 11451-11455; *Angew. Chem.* **2018**, *130*, 11622-11626; b) M. A. Silver, T. E. Albrecht-Schmitt, *Coord. Chem. Rev.* **2018**, *375*, 459-488.

[18] N. E. Brese, M. O'Keeffe, *Acta Crystallogr.* **1991**, *B47*, 192-197.

[19] S. J. Clark, M. D. Segall, C. J. Pickard, P. J. Hasnip, M. I. J. Probert, K. Refson, M. C. Payne, *Z. Kristallogr.* **2005**, *220*, 567-570.

[20] S. K. Kurtz, T. T. Perry, *J. Appl. Phys.* **1968**, *39*, 3798-3813.

[21] a) H. P. Wu, H. W. Yu, Z. H. Yang, X. L. Hou, X. Su, S. L. Pan, K. R. Poeppelmeier, J. M. Rondinelli, *J. Am. Chem. Soc.* **2013,** *135*, 4215-4218; b) Z. H. Yang, S. L. Pan, *Mater. Chem. Front.* **2021**, *5*, 3507-3523; c) M. Mutailipu, M. Zhang, H. P. Wu, Z. H. Yang, Y. H. Shen, J. L. Sun, S. L. Pan, *Nat. Commun.* **2014**, *5*, 3432.

[22] a) P. A. Maggard, T. S. Nault, C. L. Stern, K. R. Poeppelmeier, *J. Solid State Chem.* **2003**, *175*, 27-33; b) Y. L. Hu, C. Wu, X. X. Jiang, Z. J. Wang, Z. P. Huang, Z. S. Lin, X. F. Long, M. G. Humphrey, C. Zhang, *J. Am. Chem. Soc.* **2021**, *143*, 12455-12459.

[23] D. A. Kleinman, *Phys. Rev.* **1962,** *126*, 1977-1979.

[24] J. Lin, M. H. Lee, Z. P. Liu, C. T. Chen, C. J. Pickard, *Phys. Rev. B* **1999**, *60*, 13380-13389.

[25] R. He, Z. S. Lin, M. H. Lee, C. T. Chen, *J. Appl. Phys.* **2011**, *109*, 103510(1)-103510(5).

Entry for the Table of Contents

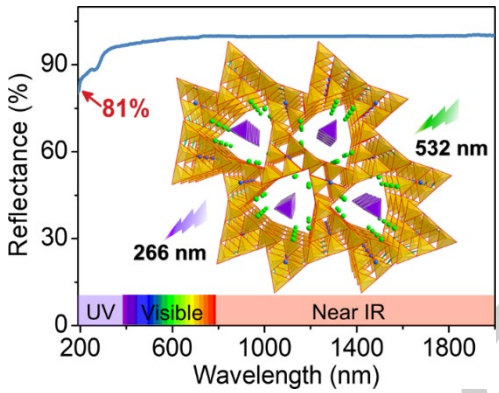

A beryllium-free deep-ultraviolet nonlinear optical hydroxyborate, $NaSr_3(OH)(B_9O_{16})[B(OH)_4]$ (NSBOH), was constructed by a covalent bond modification strategy via a facile hydrothermal reaction. Moisture-stable NSBOH is SHG-active at both 1064 nm and 532 nm, with deep-UV transparency to wavelengths below 190 nm, and good phase-matchability in the near deep-UV region, a rare combination for NLO hydroxyborates.